Contents lists available at ScienceDirect

International Journal of Mechanical Sciences

journal homepage: www.elsevier.com/locate/ijmecsci





Systematic design of Cauchy symmetric structures through Bayesian optimization

Haris Moazam Sheikh¹, Timon Meier¹, Brian Blankenship¹, Zacharias Vangelatos *,¹, Naichen Zhao, Philip S. Marcus *, Costas P. Grigoropoulos *

Department of Mechanical Engineering, University of California, Berkeley, CA 94720, USA

ARTICLE INFO

Keywords: Tailored elastic behavior Mechanical metamaterials In-situ mechanical testing Optimization Helium ion microscopy Cauchy symmetry

ABSTRACT

Using a new Bayesian Optimization algorithm to guide the design of mechanical metamaterials, we design nonhomogeneous 3D structures possessing the Cauchy symmetry, which dictates the relationship between continuum and atomic deformations. Recent efforts to merge optimization techniques with the design of mechanical metamaterials has resulted in a concentrated effort to tailor their elastic and post elastic properties. Even though these properties of either individual unit cells or homogenized continua can be simulated using multi-physics solvers and well established optimization schemes, they are often computationally expensive and require many design iterations, rendering the validation stage a significant obstacle in the design of new metamaterial designs. This study aims to provide a framework on how to utilize miniscule computational cost to control the elastic properties of metamaterials such that specific symmetries can be accomplished. Using the Cauchy symmetry as a design objective, we engineer structures through the strategic arrangement of 5 different unit cells in a 5×5×5 cubic symmetric microlattice structure. This lattice design, despite constituting a design space with 510 3D lattice configurations, can converge to an effective solution in only 69 function calls as a result of the efficiency of the new Bayesian optimization scheme. To validate the mechanical behavior of the design, the lattice structures were fabricated using multiphoton lithography and mechanically tested, revealing a close correlation between experiments and simulated results in the elastic regime. Ultimately, a similar methodology can be utilized to design metamaterials with other material properties, aspiring to control properties at different length scales, an endeavor that requires inordinate computation cost.

1. Introduction

The continued development of advanced three dimensional manufacturing processes such as multiphoton polymerization has enabled the fabrication of complex geometries with sub-micron resolution at increasingly fast rates [1,2]. Furthermore, merging spatial light modulation technologies with multiphoton lithography has resulted in the production of larger arrays with the same feature resolution [3]. Consequently, these techniques have provided the avenue to design scalable architectures, yielding bulk material properties that exceed those of natural materials [4]. These architected materials can be employed for various engineering applications such as ultralight [5–8], ultrastrong [9], reconfigurable [10], high energy absorption materials [11, 12], as well as different engineering domains such as wave mechanics [13] and optics [14]. Furthermore, the fabrication of flexible structures with tailored mechanical properties has resulted in bio-inspired

designs, inducing enhanced properties on significantly weaker bulk materials [15]. Lessons from nature can be derived from the most unexpected cases, such as the flower beetle *Torynorrhina flammea* [16] or the deep sea sponge *Euplectella aspergillum*, showing how the "optimization" of nature can lead to complex designs that resemble the features and patterns of optomechanical or purely mechanical metamaterials [17,18].

Evidently, from a structural standpoint, the lattice nature of microscale metamaterial structures has led to the predominant design strategy of truss-like structures. These structures mimic the crystalline structure and defect formation of metals and alloys [15,19–21]. These architected lattices, plate or triply periodic minimal surface structures have been revealed to provide high stiffness and increased strength at extremely low relative densities [22–25]. This is also reflected in the

E-mail addresses: zacharias_vangelatos@berkeley.edu (Z. Vangelatos), pmarcus@me.berkeley.edu (P.S. Marcus), cgrigoro@berkeley.edu (C.P. Grigoropoulos).

^{*} Corresponding authors.

¹ The authors contributed equally to this work.

plethora of results aiming specifically in the control of elastic properties, as they are determined by the stiffness tensor [26–28]. The vast majority of the literature focuses in the control of properties such as isotropy, leading to mechanical behavior independent of direction [29–31], as well as auxeticity, a property leading to negative Poisson's ratio and resilience to collapse mechanisms such as necking and barrel shape formation [32,33].

Apart from design approaches such as the addition of beam elements, and the reconfiguration of beam sizes [12,19,34], accelerating the design process and circumventing the inherent challenges of continuum modeling [35,36] has been accomplished through optimization. Several studies have attempted employing optimization techniques to obtain the elastic properties of the structure. Techniques such as topology optimization [27,37], artificial neural networks [38,39] and machine learning [40-43] have risen in metamaterial design and have steadily become a key aspect in the investigation of controlled elastic properties. Nevertheless, in these publications, the required number of evaluations to obtain the optimum is thousands, tens of thousands or even millions of data to explore the design space [27], creating a high computational cost. As a consequence, the number and type of design variables (continuous, discrete, qualitative and ordered) has to be limited and in many cases isolate the study to 2D or uniform homogeneous 3D structures to sustain a feasible computational budget. Some techniques with low computational budget using Radial Basis Function networks and Quasi-Monte Carlo methods for the interpolation of the objective functions have also been proposed [40,44-46]. In our previous work, we explored how these challenges can be successfully surpassed by the development of a novel Bayesian Optimization scheme [12]. We combined this algorithm with a new approach to model different building blocks in the metamaterial structure as states, which are discrete, qualitative design variables [12,47]. This approach required only 250 cost function evaluations, and resulted in nonuniform mechanical metamaterials with architected defects, facilitating enhanced mechanical behavior which was orders of magnitude higher than the thoroughly studied monolithic metamaterial structures [11,48]. This study aims to expand our improved Mixed-variable Multi-Objective Bayesian Optimization (MixMOBO) framework on the following fronts: (a) decrease the computational cost by an order of magnitude even with a larger number of states, rendering such exorbitant problems more accessible even with meagre computational sources using MixMOBO. (b) Design lattice structures that are nonhomogeneous in every direction, expanding the design of arbitrary metamaterials [49] to complex 3D problems.

Investigating the controlled elastic behavior of imperfect and nonhomogeneous lattices will elucidate a new approach to address such problems. However, instead of the thoroughly studied isotropy and auxeticity, this study will explore another intriguing property derived from crystalline materials, namely the Cauchy-Born Rule [50-52]. This model shows that elastically deformed states of the lattice model at the localized level are closely approximated by solutions of the continuum model. Even though this kinematic rule is based on the absence of lattice vibrations and ionic polarization, limiting its validity to describe complex phenomena in the lattice, it has been thoroughly employed as the constitutive behavior of continuum regions in multi-scale models. Thus, this fine scale is proposed to depict the real behavior of crystalline structure when the continuum description is incapable to accomplish this [53]. As it will be explained later, this rule is referred with respect to the stiffness tensor of the material as "Cauchy Symmetry". Therefore, designing mechanical metamaterials with Cauchy Symmetry will provide new metamaterial families that can be used for homogenized continua and constitutive models, enabling the fabrication of structures with homogeneous behavior.

Thus, using Cauchy Symmetry as an example of a non-intuitive design objective, we present a method to systematically tailor the mechanical behavior of architected microstructures. By building a $5\times5\times5$ microlattice structure out of five different unit cells, we yield a large

combinatorial design space. Such a design space with combinatorial or categorical variables and with an expensive-to-evaluate black-box cost function would be prohibitively expensive to optimize with conventional optimization techniques. We use our Mixed-variable Multi-Objective Bayesian Optimization (MixMOBO) algorithm [54] to optimize this large and expensive combinatorial design space. Through finite element analysis simulations, we study the mechanical response and calculate the elastic constants of the lattice which are the data required for the algorithm. To validate our results, we employ multiphoton lithography to fabricate the structures resulted by the optimization, which enables the design of complex nonuniform 3D structures. Finally, with in-situ SEM-microindentation experiments, we evaluate the validity of the optimization algorithm. Our results illuminate how complex 3D structures can be successfully optimized with a low computational budget and can lead to new types of metamaterials that can be employed for continuum modeling and controlled elastic behavior.

2. Problem setup

2.1. Modeling of Cauchy-Symmetric structures

The Cauchy-Born rule relates the position of atoms in a crystal to the overall strain of the medium [52]. Assuming that the potential energy of the lattice is a function of the distance between the atoms, or in lattice metamaterials, the nodes, the elastic stiffness tensor C can be obtained through the second derivative of the potential energy with respect to the strain. Databases possessing millions of geometries to describe the mechanical properties of truss metamaterials as a function of the lattice node locations have been reported [27], indicating that such an assumption can be valid as long as higher gradient elasticity is not dominant [36]. However, the particular form of the potential energy in the Cauchy-Born rule can lead to an additional symmetry in the stiffness tensor, defined as "Cauchy Symmetry". This additional symmetry reduces the number of independent elastic constants in the structure, leading in some cases to unphysical results as in a triclinic material. However, while the number elastic independent variables of bulk materials cannot be physically reduced, the arrangement of beam members in the metamaterial structure can result in the control of the elastic constants [55].

A particular case of interest is that of metamaterials possessing cubic symmetry, since the vast majority of thoroughly studied structures such as the Diamond, the Octet Truss, and the Kelvin foam exhibit it [56]. In this reduced form, the effective stiffness tensor has only three independent elements: C_{11} , C_{12} , and C_{44} , where C_{11} and C_{12} are stiffness components of normal stress and C_{44} specifies the shear modulus of a cubically symmetric structure. This correlation between stiffness elements and loading mode are conveyed in Fig. 1. However, Cauchy-Symmetry is obtained in a cubic material when $C_{12} = C_{44}$. Accordingly, the cost function to minimize is defined as

$$f(\mathbf{w}) = |C_{12} - C_{44}| \tag{1}$$

This requirement will set the framework to define the problem and optimize it as it will be discussed in the next section.

2.2. Cauchy symmetry problem setup

The objective of this work is to design a nonmonolithic microlattice composed of discrete unit cells that is Cauchy Symmetric. Fig. 2 depicts the process used to identify and validate a near-optimal structure. Throughout this process we use five different unit cells, shown in Fig. 2a, labeled A, B, C, D or E. For simplification, we choose unit cells that have cubic symmetry so that they can be systematically joined together to create a bulk microlattice. The unit cells are all face-centered and contain nodes in the center of all six faces. This enables arbitrary and independent combination of unit cells in a lattice and prevents overlapping of different beam elements. Each unit cell is $10\,\mu m$

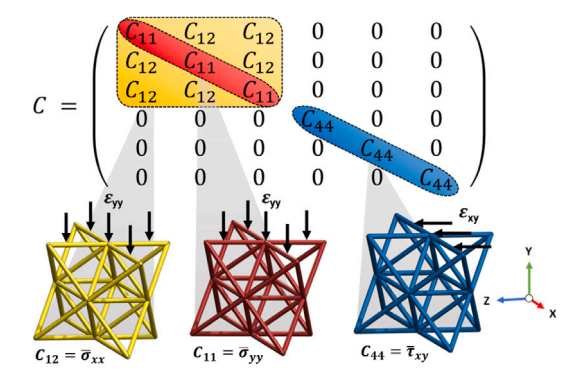


Fig. 1. The stiffness matrix of a cubic symmetric unit cell can be described by three independent stiffness components which corresponded to the stress components orthogonal to the direction of strain (left) the stress components in the direction of loading (middle) and the shear modulus (right).

 \times 10 µm \times 10 µm, which is compatible with the feature resolution of the multiphoton lithography (MPL) apparatus. These unit cells are positioned in a 5 \times 5 \times 5 array. Thus, the layout scheme of unit cells depicted in Fig. 2b was selected. The micro lattices consist of an outer "shell" (Layer 1, with 5 \times 5 unit cells), a middle layer (Layer 2, with 3 \times 3 unit cells), and the inner core unit cell (Layer 3, with 1 \times 1 unit cell). The ten positions 1–10 of the different layers ensure that the boundary condition of cubic symmetry is fulfilled. Accordingly, the same unit cells must be positioned at locations with the same number. Thus, specific microlattice structures can be described by a unique 10 component ω -vector. For instance, the corresponding vector for the microlattice shown in Fig. 2a is $\omega_{2a} = \left[EEBEEDCCAC \right]$.

This layout scheme was strategically chosen to provide two key benefits. The first benefit is that it reduces the stress tensor to three independent stiffness values which simplifies the number of simulations and mechanical tests required to probe the stiffness values. The second benefit is that it substantially reduces the number of possible combinations of lattices. With this restriction, the design space reduces from 2.3*10⁸⁷ states to 9765625. Even though the searched design space potentially has multiple sufficiently low values of the cost function, the reduction in the dimensionality of the design space should still significantly reduce the number of function evaluations required. In addition, it is important to state that even though symmetries in the lattice structure will also decrease the design space, the optimization algorithm determines the overall number of required evaluations based on the overall size of the design space.

Fig. 3 shows the pseudocode for the optimization utilized to find a Cauchy-Symmetric microlattice. Fabricating and physically testing structures is a very expensive process (fabrication, sample preparation, testing and validation). In addition, the noise caused my the mechanical testing will also affect the required number of data. Therefore, finite element analysis is used as a proxy for calculating stiffness components for the cost function in our MixMOBO algorithm, which is detailed in [54]. To converge to a near-optimal solution we input the calculated stiffness values from our finite element code into our MixMOBO algorithm. The optimization of lattice properties requires that this computation must be done repeatedly. In turn, even this more timeeffective method remains prohibitively expensive to search the entire design space or employ other optimization techniques that still require thousands of function calls. As it will be explained in the following sections, despite the fact that the problem presented in this study is linear elastic, the high computational cost is derived by the generation of the CAD of the structure and the iterations of the optimization as the number of data increases. A deviation of less than 1% between C_{12} and C_{44} is defined as tolerance for an optimal solution. Once our algorithm converged on an acceptable solution, the optimum was fabricated and

mechanically tested (further information about the mechanical testing process is provided in Materials and Methods).

The material that was used was the hybrid organic–inorganic Zr-DMAEMA [(2-dimethylaminoethyl) methacrylate] (further details about the fabrication and the material properties are provided in Materials and Methods). Based on previously conducted work [47], the stiffness values measured by mechanical testing can only be repeatedly measured within the elastic regime, since the photoresist material is highly sensitive in the plastic domain due to variations in the fabrication parameters. To incorporate the noise caused by fabrication imperfections and the experimental measurement, a 0.005 noise variance (7% standard deviation) is built into the test function based on previously reported results [12]. Mechanical testing and structural analysis are conducted inside a scanning electron microscope (SEM).

2.3. Bayesian optimization

Optimization for expensive black-box functions involving categorical or mixed variables is an area of active research. For such complex problems, Bayesian optimization (BO) uses a small number of function calls compared to other optimization strategies, proving to be extremely efficient [57]. A large range of these problems require optimizing combinatorial or categorical design spaces. Bayesian optimization is a natural candidate for architected material design [12,58–62], hyperparameter tuning for machine learning algorithms [63–65] and drug design [66,67]. However, for problems such as the design of architected materials, the design space can include categorical or ordinal variables [12].

Bayesian optimization (BO) has been thoroughly studied for continuous design spaces with minimum number of expensive function calls [57,68]. Albeit the success of continuous Bayesian optimization strategies, combinatorial problems remain an area where new and more versatile approaches are developed. The inherent continuous nature of Gaussian processes (GP) renders categorical variables challenging.

In our past work, detailed in [54], a Mixed variable, Multi-Objective Bayesian Optimization (MixMOBO) algorithm was developed. This is a generalized framework that can address categorical problems and can optimize a noisy black-box function with a small number of function calls. A categorical variable Bayesian optimization algorithm was employed (previously known as Evolutionary Monte Carlo Simulations, EMCS) for the design of an architected metamaterial that possesses maximum strain-energy density [12]. The fabrication and testing of this new material showed that it had a normalized strain energy density that is 10⁴ times greater than existing unblemished microlattice structures reported in literature [12]. The principal improvement of the algorithm used in the present study is the utility of a hedge strategy which hedges acquisition functions. This approach uses a set of acquisition functions instead of a single one, rendering the algorithm much more efficient and versatile than EMCS. MixMOBO is further detailed in Section 3.2.

3. Materials and methods

3.1. CAD modeling and FEA design

All of the structures called by the optimization algorithm were manually designed using SOLIDWORKS. All FEA simulations were performed with the multipurpose finite element code ANSYS (Workbench 18.0). The following beam lattice properties were used in the FEA: 1.281 GPa elastic modulus and 0.4999 Poisson's ratio. The structures were meshed with 10-node, tetrahedral finite elements. Each structure roughly contained between 100,000 and 900,000 nodes. The average element size was selected by conducting a mesh convergence study. Even though for the case of linear elasticity the use of beam elements would decrease the computational cost of the FEA analysis, for the present study the required number of simulations is too small and

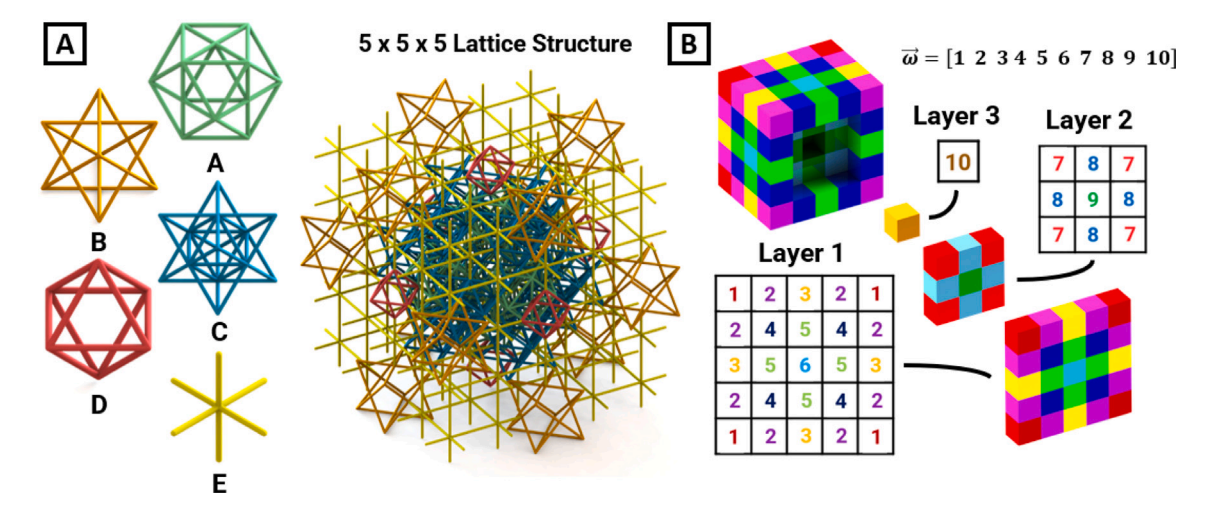


Fig. 2. (a) Five types of cubic unit cells, labeled A-E, used to construct a $5 \times 5 \times 5$ lattice. Unit cells are all face-centered cubic geometry to ensure compatible connectivity within the lattice (b) Unit cells are placed together into three layers that are cubic symmetric. Unit cells of the same type are placed into one of 10 positions, labeled 1–10, which are elements of the ω -vector. Layer 1, located on the outside of the structure is composed of 5×5 unit cells. Layer 2 is the middle layer and is composed of 3×3 unit cells, and Layer 3 is a singular unit cell located in the center of the microlattice.

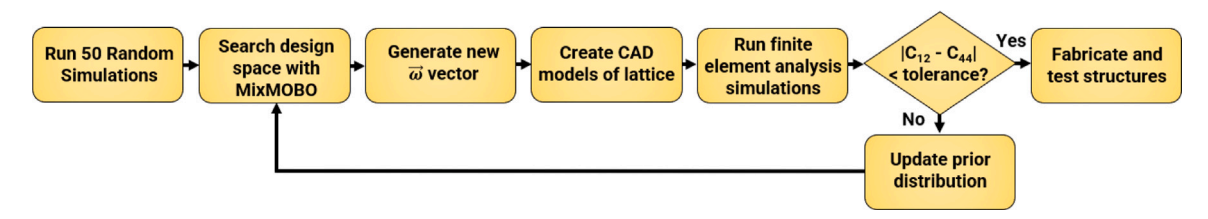


Fig. 3. Pseudocode beginning with the selection of 50 initial random microlattices. Afterwards the process iteratively loops between (i) application of the MixMOBO algorithm to choose new parameters and (ii) the modeling, simulation, and evaluation of the Cauchy-symmetry cost function. Once a microlattice with sufficiently small cost function value is found, the iterative loop ends and the optimal design is fabricated and tested to validate its properties.

the total computational time is dictated by the CAD generation and the iteration process. To put this into perspective, beam elements in the range of 100,000 to 200,000 nodes require 73% less CPU time compared to solid tetrahedral elements with 6% difference in the value of the elastic constants using the same hardware system (1.5 s). However, this is only 0.56% of the total time of each iteration if the time of the optimization process and CAD generation is included. Therefore, the computational cost is dominated by the number of iterations as in every stochastic optimization scheme. Nonlinear problems would require computational time commensurate with the optimization iteration and would necessitate more efficient simulation techniques. However, in the present study the principal challenge is to minimize the number of iterations by reducing the number of required data points instead of the FEA time. For uniaxial compressive testing, an infinitely stiff plane attached to the top surface of the structure was displaced downwards and C_{12} was calculated by averaging σ_{xx} (Figure S1 in supplementary information (SI)) across all elements. For shear testing and a vertice on the structure was displaced laterally and C_{44} was calculated by averaging τ_{xy} across all elements (Figure S2 in SI). In both cases, the bottom face of the structure was attached to the substrate and fully constrained. This methodology has been employed before for the precise calculation of the polar stiffness map of structure, leading to a close correlation between theoretical and experimental results [69]. Further information on the applied boundary conditions and FEA models can be found in SI.

3.2. Optimization (MixMOBO)

For minimizing the objective, we pose the categorical variable problem as:

$$\mathbf{w}_{opt} = \operatorname{argmin}_{\mathbf{w} \in \mathcal{W}}(f(\mathbf{w})) \tag{2}$$

 $f(\pmb{w})$ is the objective to be minimized, and $\pmb{w} \in \mathcal{W}$ is a categorical variable vector, defined as $\pmb{z} = [w_1, \dots, w_m]$ for m total variables. \mathcal{W} is the combinatorial space. Each categorical variable takes a value $w_j \in \{C_1, \dots, C_j\}$ from C_j unordered categories (that cannot, by definition, be ordered on the real-number line).

For practical engineering problems f(w) can be extremely expensive to evaluate. In addition, gradient based algorithms cannot be used for combinatorial problems. The difficulty of optimization is also exacerbated due to the dimensionality of the design space making some problems intractable to optimize using conventional optimization techniques. For every iteration in the Bayesian optimization process, a surrogate model g, is fit over the data set $\mathcal{D} = \{(w_1, f(w_1)), \dots, (w_i, f(w_i))\}.$ Here i is the total number of points evaluated until the ith iteration. Gaussian processes (GP) are usually used as the surrogate models. Once the surrogate surface has been fit to the data, the surrogate surface is explored to determine which point has the highest probability of finding the optimum (exploitation) point as well as improving the fit of the surrogate surface (exploration). An acquisition function is used to balance the exploitation and exploration trade-off and determine the next point w_{i+1} for evaluation with f. w_{i+1} is then evaluated using fand appended to the data set, $\mathcal{D} = \mathcal{D} \cup (w_{i+1}, f(w_{i+1})).$ The process is repeated until the evaluation budget for f or the global optimum is reached.

For combinatorial or mixed variable problems, conventional Bayesian optimization techniques cannot be used due to the smooth nature of GP. In our previous work [12], EMCS was introduced, a Bayesian optimization algorithm for combinatorial variables using Stochastic Monte-Carlo (SMC) acquisition function. In the current work, we use MixMOBO, a mixed variable algorithm we developed to optimize find a Cauchy-Symmetric structure within the design space. It also uses HedgeMO, a hedging strategy introduced as part of MixMOBO that

Table 1

| Name | Objective functions | Notes |
|---|---|--|
| Encrypt. Spherical Encrypt. Rastringin | $\begin{split} f(\boldsymbol{w}) &= w_i^2, w_i \in (-10, 10) \\ f(\boldsymbol{w}) &= [10 + w_i^2 - 10\cos(2\pi w_i)], w_i \in (-5.12, 5.12) \end{split}$ | Convex Non-convex |
| Encrypt. Syblinski-Tang | $f(\mathbf{w}) = \frac{w_i^4 - 16w_i^2 + 5w_i}{2}, w_i \in (-5, 5)$ | Non-convex |
| Encrypt. Amalgamated | $\begin{split} f(\boldsymbol{w}) &= \sum_{i=1}^{D_i} g(w_i) \\ &= \begin{cases} -sin(w_i), \text{ if } k = 0, \ w_i \in (0,\pi) \\ \frac{w_i^n - 16w_i^n + 5w_i}{2}, \text{ if } k = 1, \ w_i \in (-5,5) \\ w_i^2, \text{ if } k = 2, \ w_i \in (-10,10) \end{cases} \\ g(w_i) &= \begin{cases} [10 + w_i^2 - 10cos(2\pi w_i)], \text{ if } k = 3, \ w_i \in (-5.12,5.12) \\ [100(w_i - w_{i-1}^2)^2 + (1 - w_i)^2], \text{ if } k = 4, \ w_i \in (-2,2) \\ - cos(w_i) , \text{ if } k = 5, \ w_i \in (-\pi/2,\pi/2) \\ w_i, \text{ if } k = 6, \ w_i \in (-30,30) \end{cases} \end{split}$ | Non-convex, Non-uniform, Anisotropic |
| | $k = mod(i-1,7), i = 1, \dots, n$ | |

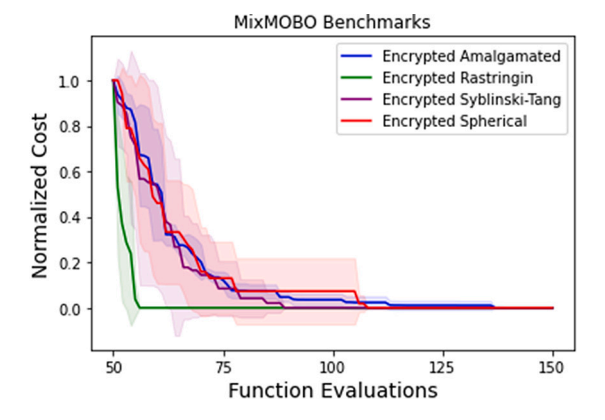


Fig. 4. Benchmarks for MixMOBO. The vertical axis is the Normalized Cost, defined as *(global optimum - current optimum)/(global optimum - random sampling optimum)* and the horizontal axis is the number of black-box function evaluations.

uses a portfolio of acquisition functions rather than a single one. Hedge algorithms have proven to be efficient in dealing with a diverse set of problems since they do not rely on a single acquisition function which might affect the efficiency of the BO algorithm [70].

To test the efficacy of MixMOBO for our problem, we test MixMOBO on a range of test functions with the same design space as our problem, i.e. 10 categorical variables with 5 categories for each variable. These tests demonstrate the number of function calls that would be necessary to optimize a design space of this size. MixMOBO is run 5 times for each test function to ensure reproducibility with 50 initial random data points. Encrypted Amalgamated, Encrypted Rastringin, Encrypted Syblinski-Tang, and Encrypted Spherical are used as the test functions. These test functions are commonly used for performance benchmarking of optimization algorithms [71] and have been modified for testing categorical variables.

All test functions are defined to be minimized. Analytical test functions are generally not able to mimic mixed variables. Therefore, a method to 'Encrypt' the test functions is formulated, which renders them suitable for mixed variable problems. The categorical variable dimension of the test function is first discretized into the required number of categories by equally spaced points within the bounds. A random vector for each categorical variable is generated which scrambles or 'encrypts' the indices of these values. Thus, random landscapes are created, same as categorical variables with a latent space. The optimization algorithm only sees the encrypted space and the random vector is only used when evaluating the black-box function. For ordinal variables, the design space is discretized.

A new test function is also defined, called the *Amalgamated function*, a piece-wise function formed from commonly used analytical test functions with different features. More details on these functions are provided elsewhere Tušar et al. [71]. The Amalgamated function is non-convex and anisotropic, unlike conventional test functions where isotropy can be exploited. The other test functions used in Encrypted mode are commonly used for testing optimization algorithms [71] and are detailed in Table 1.

For categorical variables, equally spaced points are taken within the bounds defined above. In the present work, $D_t=10$ space categorical variables is used with 5 states, each similar to our lattice optimization problem. The results of our benchmarks are shown in Fig. 4. The plots show Normalized Cost, defined as (global optimum - current optimum)/(global optimum - random sampling optimum) versus number of black-box function evaluations, with the Normalized global minima at 0. The mean Normalized Cost of 5 runs for each test function and the standard deviation is plotted. For each test function run, global optimum is found within 150 function calls, demonstrating the efficacy of the MixMOBO setup.

3.3. Fabrication

The microlattice structures were fabricated with a hybrid organicinorganic resin Zr-DMAEMA (30 wt%). The resin is composed of 70 wt% zirconium propoxide and 10 wt% (2-dimethylaminoethyl) methacrylate (DMAEMA) (Sigma-Aldrich). The structures for mechanical testing were fabricated by sub-micron resolution direct femtosecond laser writing, which uses MPL and the aforementioned photoresist for high-resolution fabrication. The basic optical system consists of a FemtoFiber pro NIR laser emitting 780 nm wavelength, with a pulse width of 100 fs, and a repetition rate of 80 MHz. The local photopolymerization of the photosensitive material was accomplished with a 100×microscope objective lens (Plan-Apochromat 100×/1.40 Oil M27, Zeiss). The laser output energy for the fabrication was measured before the objective lens at 4.2 mW, and the scanning speed used was set to 20 μ m/s. The resin sample is attached to a stage with both piezo and servo elements with movements in the XYZ directions.

3.4. Mechanical testing

Compression and shear tests were performed *in situ* with a nanoin-dentation apparatus (PI 87 SEM PicoIndenter, Hysitron) mounted inside the chamber of a scanning electron microscope (SEM) (FEI Scios 2, Thermo Fisher Scientific). A molybdenum flat tip indenter (model 72SC-D3/035 (407A-M) Probing Solutions, Inc.) with a diameter of 70 μm is applied in all mechanical tests. The glass substrates on which the microlattices are fabricated are fixed onto an SEM pin stub mount

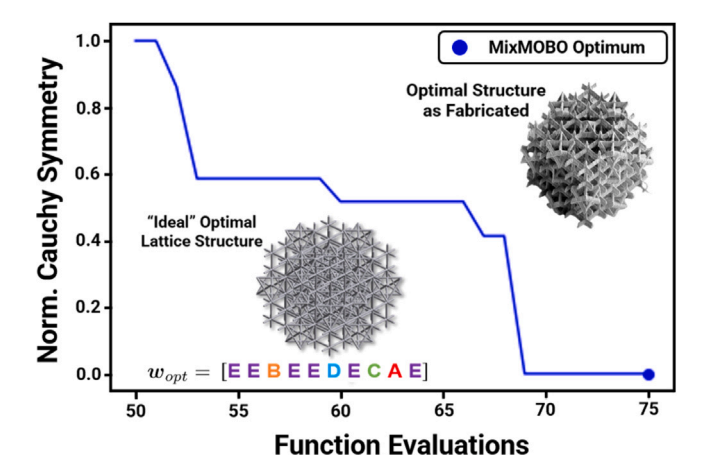


Fig. 5. Optimization progress for Cauchy-Symmetric structures. The vertical axis is the Normalized Cauchy-Symmetry, defined as *current optimum/random sampling optimum* and the horizontal axis is the number of black-box function evaluations.

(TED PELLA) with PELCO® Pro C100 Cyanoacrylate Glue (TED PELLA). Test structures for compression testing are aligned such that the top face contacts the indenter tip while the side profile is imaged by the electron beam. Test structures for shear testing are aligned such that a side face with a flat bar attached on the side contacts the indenter and the top is imaged. Each structure was deformed at a rate of 250 nm/s, and to ensure repeatability, 4 tests were performed on each structure. These tests are preformed using the same methodology reported in our previous studies [12]. While similar in-situ SEM indentation experiments have also been reported elsewhere [20,22,23,26,44], a frame by frame juxtaposition of the deformation with the force displacement curve is conducted to identify the critical deformation events of the test (i.e. post contact, buckling or fracture).

4. Results

4.1. Convergence of the algorithm

Based on 50 random sampling data of the search space, the mean cost function value and variance of search space are $\bar{x}=1.038$ and $s^2=0.190$, whereas the cost function value of an optimal cauchy symmetric structure is equal to zero. The convergence of the algorithm is summarized in Fig. 5. A sequential history of Normalized Cauchy-Symmetry is plotted, which is defined as: (current optimum/random sampling optimum). The random sampling optimum is the value of the objective function obtained after the initial 50 random evaluations. It is noted that despite the fact that the design space is comprised of almost 10^7 structures, the algorithm converged after 69 function evaluations, which is at least 3 orders of magnitude lower compared to other optimization schemes reported elsewhere [54]. The structure, as it is mathematically described in Fig. 2b is shown in Fig. 5 and has the following sequence $w_{opt} = [EEBEEDECAE]$.

It is noted that this structure does not have any specific pattern or layer arrangement that shows some periodicity or uniformity in specific directions. To experimentally validate the optimized structure, it was fabricated by the MPL apparatus provided in the previous section. Specifically, to control the uniformity of the cross section of the structures, all tested structures were made from the same batch of resin, printed within a 24 h period of each other, and the laser power, scan speeds and beam alignment held constant. Likewise each beam member was fabricated using multiple passes of the laser beam at the same location.

4.2. Properties of optimum structure

To extract the elastic constants from the experimental results, the directional elastic properties were obtained following the methodology that is provided elsewhere [72]. Specifically, the directional Young's Modulus, Poisson's ratio and Shear Modulus are provided by the following equations:

$$E(\mathbf{n}) = 1/S_{11}' \tag{3}$$

$$G(\mathbf{n}, \mathbf{m}) = 1/S'_{\Delta\Delta} \tag{4}$$

$$v(\mathbf{n}, \mathbf{m}) = -S'_{12}/S'_{11} \tag{5}$$

where **n** is the direction normal to the loading, **m** is the perpendicular direction in the shear plane, S'_{11} , S'_{12} and S'_{44} are the tensor products of the vectors **n** and **m** with the compliance tensor C^{-1} . Based on these definitions, for the direction **n** = [100] and **m** = [010], the ratio of the elastic constants C_{12} and C_{44} is given by the following equation:

$$C_{12}/C_{44} = \frac{F\varepsilon_{22}\varepsilon_{12}}{\varepsilon_{11}^2 T(1 - \varepsilon_{22}/\varepsilon_{11})(1 + 2\varepsilon_{22}/\varepsilon_{11})}$$
 (6)

where F is the measured force during compression, T is the measured force during shear, ε_{11} is the strain in loading direction during compression, ε_{22} is the strain in the perpendicular direction during compression and ε_{12} is the strain during shear. To obtain the measurements for the aforementioned quantities, compression and shear test were conducted. The fabricated optimal structure is presented in Fig. 6(a) (isometric view) and (b) (top view), captured in the Helium Ion Microscope, enabling high resolution imaging and large depth of focus to observe the internal nonuniformity.

Characteristic force—displacement curves for the two types of experiments are shown in Fig. 7(a). Through the experimental curves and the video recordings provided in the supplementary material (Video A for compression and Video B for shear), the parameters of Eq. (6) can be obtained. A representative frame of the compression measurement and a shear measurement are shown in Fig. 7(b) and (c) respectively. For a set of shear tests and compression tests, the ratio C_{12}/C_{44} was found equal to 0.9752 ± 0.0035 , a result close to the theoretical estimate of the FEA simulations which is 1.

5. Discussion

It was demonstrated how the stiffness tensor of the lattice structure was controlled, such that the Cauchy symmetry rule was accomplished using our MixMOBO scheme. The versatility and efficiency of the algorithm is reflected on the minuscule number of simulations required to obtain the optimum. Specifically, the optimum structure was obtained using 69 function calls to calculate the elastic behavior of the lattice. This is a result of the hedge strategy, which enabled us to converge to a solution in a lower number of simulations compared to previous work [12] and two or three orders of magnitude less compared to other problems using other optimization schemes [73-75]. As a reference, a genetic algorithm would have required a number of function calls at least three orders of magnitude greater to optimize a similar problem [54]. Furthermore, since this algorithm is able to work with mixed variables (a mixture of categorical, discrete and continuous variables) and multi-objectives, one could imagine expanding this framework to a variety of different types of problems.

The structure possessing the Cauchy symmetry rule from a sample of approximately 10^7 geometries does not show any inherent pattern that could be predicted by intuition or mechanical principles. This result highlights the necessity of optimization for the design of nonmonolithic structures, but also the versatility of MixMOBO for black box and extortionate problems. Future work should focus on the utility of mixed variables frameworks for monolithic structures that also possess nonuniform thickness [27].

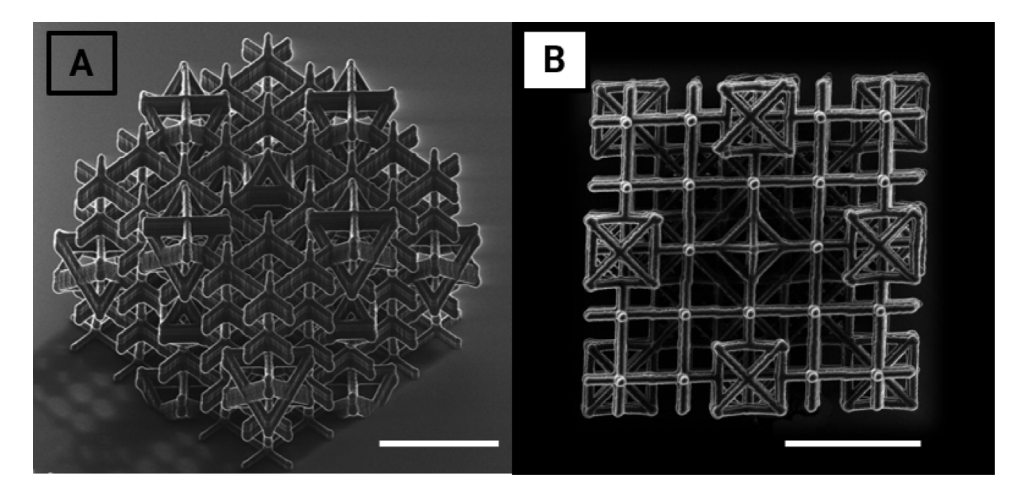


Fig. 6. (a) Orthogonal view of the Cauchy Symmetric structure taken in a helium ion microscope. (b) Top view of structure highlighting with a large depth of focus to resolve internal beam members. Scale bars are both 20 µm.

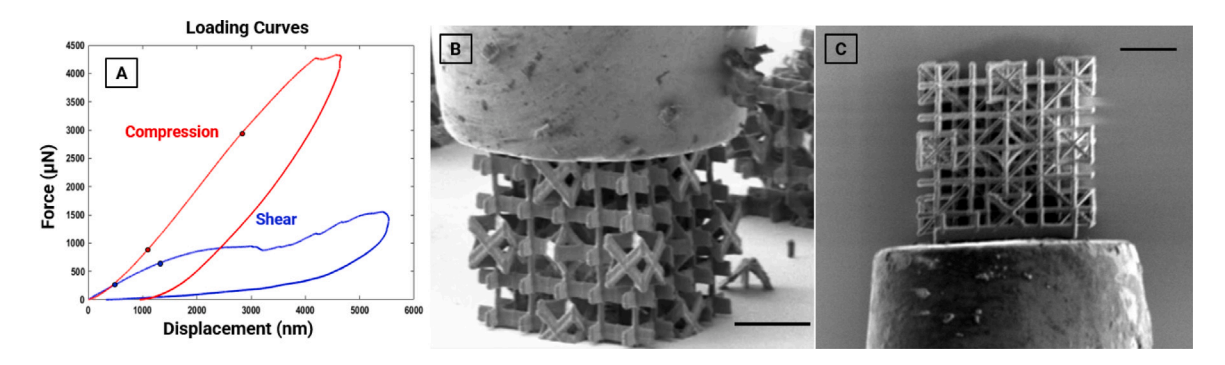


Fig. 7. (a) Mechanical loading response curves of the optimal Cauchy Symmetric lattice structure measured using a PI-87 Picoindenter. Points are added to both curves to identify slopes that can be employed for the validation of the cost function. (b) Representative frame of the compression measurement. The indenter applies a compressive load to the structure in the lateral direction. (c) Representative frame of the shear measurement. The indenter is attached to the bar that is fabricated on the edge of the structure, applying a shear load to the geometry. Scale bars are both $20 \mu m$.

Regarding the mechanical performance of the optimal structure, a juxtaposition of the force-displacement curve with the video caption also demonstrates the reverberations of Cauchy Symmetry to the mechanical performance. These results are depicted in Fig. 8. In previous work the introduction of architected defects led to controlled densification and tailored buckling, but the small number of unit cells that can be realized by the MPL also leads to boundary effects [7,20,26]. However, a frame by frame comparison of the compression measurement shows that whole array of lattices follows the overall strain of the medium (Fig. 8a), without substantial localized failure events as they had been observed before [12]. While this is one of the necessary assumptions for the Cauchy–Born rule to be valid in a crystalline material, the observation of this effect to the optimal array signifies the potential utility of such structures for the design of homogenized microscale lattices. In addition, during a loading mode such as shear at the edge of the structure, localized buckling and post contact phenomena are shown (Fig. 8b), leading to a serrated profile in the force-displacement curve and densification. The buckling deformation is dominant on the $\pm 45^{\circ}$ plane. This same mechanism was observed under compression in lattice structures with architected defects or different types of unit cells [12] and resembles the formation of mechanical twinning during shear that has been investigated when the Cauchy-Born rule is satisfied [76]. The consequence of this mechanism in shear loading mode can result in architected materials with improved tribological properties, enhanced post linear elastic mechanical performance and strain hardening [47].

Furthermore, future work should focus on the exploration of the design space with different types of unit cells. Different unit cells will significantly increase the design space. For instance, utilizing 6 or 7

types of different unit cells instead of 5 leads to a design space comprised of 60 466 176 and 282 475 249 lattice structures respectively. Moreover, increasing the size of the lattice increases the size of the design space. While a $5\times5\times5$ 3D cubic lattice has 10 design variables, it can be shown that the number of design variables increases each two steps. A $6\times6\times6$ array still has 10 design variables, while a $7\times7\times7$ and $8\times8\times8$ have 20 design variables. Utilizing 5 different types of unit cells will lead to a design space of approximately 9.53 * 10^{13} lattices. Therefore, different strategies should also be explored to decrease the computational cost for such design spaces and identify different methodologies to define the design space. To this end, the generation of data-bases to easily extract specific geometries and use for the optimization algorithm would be a versatile tool to automate this process.

Future work should also focus on the effect of such lattices on the vibrational behavior of the structure and the effect of the Cauchy symmetry on the dispersion curves of the lattice. This investigation will reveal how the tailored stiffness tensor will affect the wave propagation to the medium and control the energy absorption in the materials, creating band-gaps and deformation isolation as it has been reported elsewhere [77]. This effect is related with the directional stiffness of the material, which controls the slope of the dispersion curve. The directional stiffness map of the Cauchy symmetric optimum compared with the monolithic structures (i.e. structures comprised of only one type of unit cell) can be calculated by the following equation:

$$E(n) = \frac{1}{(n \otimes n) : C^{-1}(n \otimes n)}$$
(7)

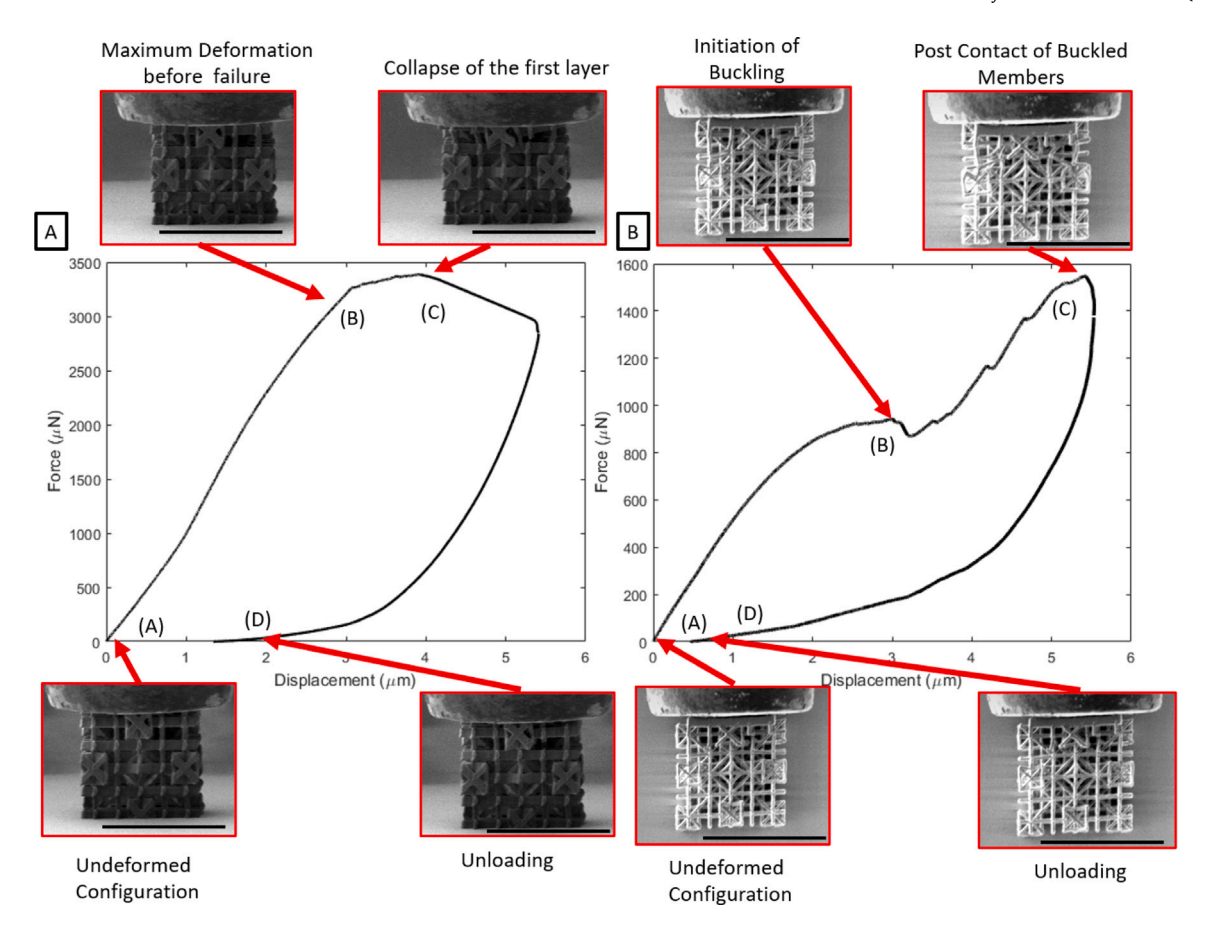


Fig. 8. In situ analysis of the force displacement curves for compression and shear. (a) The response of the structure during compression shows a smooth linear response without discernible boundary effects (stage A–B), until the critical failure load is reached and the first layer collapses (stage C), leading to permanent deformation (stage D). (b) The response of the structure during shows the transition from linear behavior to instability and buckling of the lattice members (stage A–B), which result the initiation of microbuckling phenomena and densification, creating a serrated profile (stage B–C) without extensive permanent deformation (stage C–D). The black scale bar is 50 μm.

where n is the normal vector of the loading direction and \otimes denotes the tensor product. The various maps are presented in Fig. 9. To quantify the variance of the stiffness for the different structures, the Zener ratio A is used [69], defined as

$$A = 2C_{44}/(C_{11} - C_{12}) (8)$$

The Zener ratio is a metric that shows how a cubic structure deviates from isotropy. Structures with A = 1 are isotropic, despite having cubic symmetry. Even though none of the monolithic structures is either Cauchy symmetric or isotropic, it is observed that the Cauchy symmetric Optimum has Zener ratio larger than the monolithic structures $(A = 0.7 \text{ compared to } 0.03 \le A \le 0.57 \text{ for the monolithic states}).$ This is a counter intuitive result considering that the Optimum is a combination of unit cells from the different monolithic structures. It is also noted that the monolithic state E is the only one that has f(w)closer to 0 compared to the other monolithic states ($f(w)_E = 0.54$). All of the others have 3-4 times larger value for the cost function. However, even though the optimum has several positions with state E (Fig. 5), Cauchy symmetry is accomplished by using states that deviate far more from the optimum compared to E. These results highlight how Bayesian Optimization can reveal these optimal points that cannot be derived by intuition. In addition, due to the versatility of our MixMOBO scheme, multi-objective optimization problems that search for Cauchy Symmetry combined with isotropy, auxeticity or controlled band gap ranges should be further investigated. This will explain how states that deviate from the respective cost functions can create optimal structures if combined together in a 3D configuration.

For the experimental validation of these effects, experimental techniques such as heterodyne interferometry and laser Doppler vibrometry

can be employed to record a reflection of a laser beam through time and calculate the velocity of the vibration through the medium [78]. These results illuminate the necessity of larger scale printing that can capture the required feature resolution of the lattice members fabricated by MPL and can facilitate a tailored mechanical performance in the bulk material. To achieve this, more advanced additive manufacturing techniques such as projection lithography [3] can increase the printing area and also reduce the fabrication time to efficiently produce mesoscale samples. Therefore, these structures possessing Cauchy symmetry will lead to macroscale structures with simpler constitutive behavior and controlled post contact deformation as it was shown on the experimental results. While other lattices possess controlled directional stiffness, such as orthotropic or hexagonal [56], Cauchy symmetry lattices can pave the way for the control of more complex phenomena. Thus, models with a smaller number of parameters would enable the control of coupling shear deformation, warping and twisting similar to higher gradient models [36,79-81]. This would lead to materials that could also be used to optimize the complex deformation of thin-walled structures with enhanced stiffening, high energy absorption and reversible deformation [7,82], as it has been investigated in other theoretical studies regarding the deformation of hollow nanotubes [83]. These results will accentuate the systematic optimization and utility of hollow microscale structures for high energy absorption materials used in biomimetic design and tissue engineering.

6. Conclusions

In this work, a new Bayesian optimization scheme, MixMOBO, was used for the design of nonmonolithic architected materials described

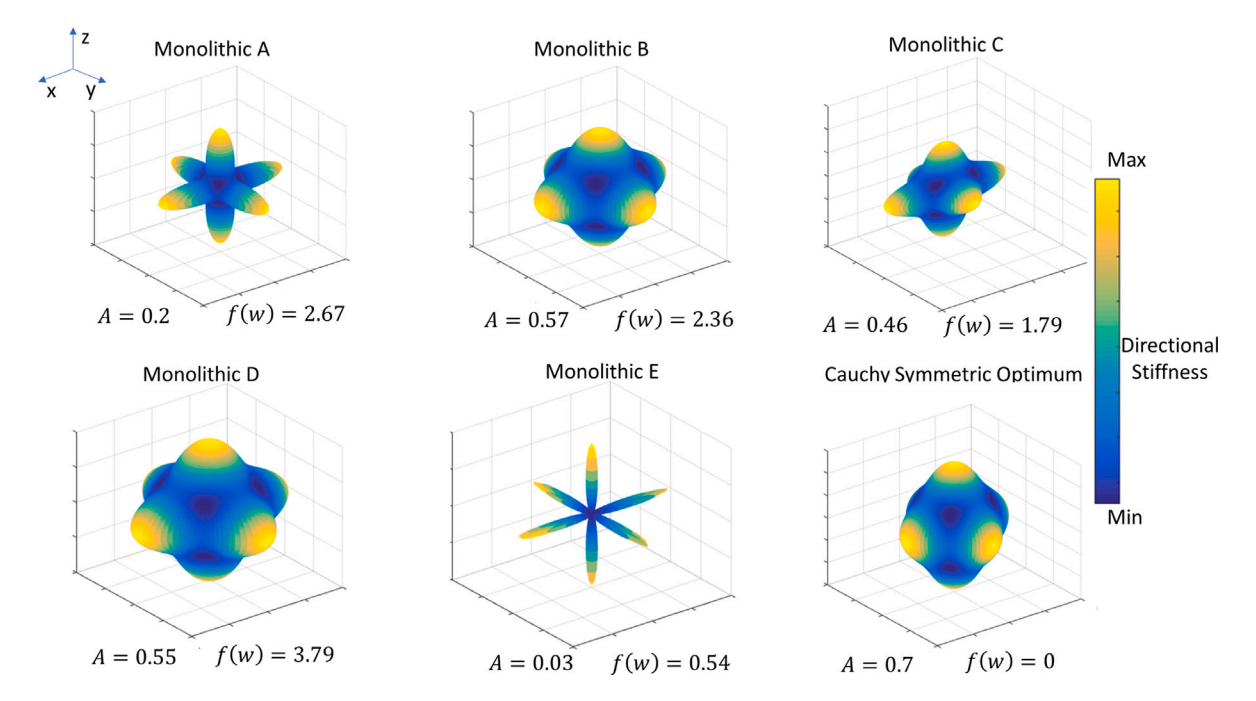


Fig. 9. Directional stiffness map of the monolithic structures and the Cauchy symmetric Optimum obtained by the Bayesian optimization algorithm. It is observed that none of the monolith structures is close to Cauchy symmetry. However, their combination provides a Cauchy symmetric structure. In addition, the Cauchy symmetric optimum has Zener ratio larger than the monolithic structures, a result counter-intuitive considering that the optimum is a combination of the five different states A through E configured in the 3D space.

by discrete and qualitative design variables. Utilizing 69 data points, the optimum of the structure that possesses Cauchy symmetry was obtained in a design space of 5¹⁰ structures. Utilizing MPL and insitu mechanical testing for compression and shear, it was revealed that the structure's mechanical response shows the formation of shear planes and controlled buckling and a smooth strain, alluding how the assumptions of Cauchy–Born rule in the crystal lattice can be harnessed for the controlled mechanical performance of mechanical metamaterials. These results elucidate how the mitigation of the computational cost can pave the way for the exploration of exorbitant design spaces and the strategic design of architected nonmonolithic materials with tailored mechanical performance.

CRediT authorship contribution statement

Haris Moazam Sheikh: Data curation, Formal analysis, Investigation, MixMOBO methodology, Software, Validation, Writing – original draft. Timon Meier: Data curation, Formal analysis, Investigation, Methodology, Software, Validation, Visualization, Writing – original draft, Writing – review & editing. Brian Blankenship: Data curation, Formal analysis, Investigation, Methodology, Software, Validation, Visualization, Writing – original draft, Writing – review & editing. Zacharias Vangelatos: Conceptualization, Data curation, Formal analysis, Investigation, Methodology, Software, Validation, Visualization, Writing – original draft, Writing – review & editing. Naichen Zhao: Data curation, Investigation, Methodology, Software, Validation. Philip S. Marcus: Funding acquisition, Project administration, Resources, Supervision, Writing – review & editing. Costas P. Grigoropoulos: Funding acquisition, Project administration, Resources, Supervision, Writing – review & editing.

Declaration of competing interest

The authors declare that they have no known competing financial interests or personal relationships that could have appeared to influence the work reported in this paper.

Data availability

Data will be made available on request.

Acknowledgments

Brian Blankenship acknowledges support by the US National Science Foundation Graduate Research Fellowship under Grant No. (DGE 2146 752). SEM images were taken with the Scios 2 DualBeam and HIM images were taken with the Zeiss ORION NanoFab both available at the Biomolecular Nanotechnology Center of the California Institute for Quantitative Biosciences, UC Berkeley. We acknowledge Prof. Hosemann for use of the PI-87 Picoindenter and Frances Allen for her guidance and expertise on HIM imaging.

Funding

Support to this work by the US National Science Foundation under grant 2124826 is gratefully acknowledged.

Appendix A. Supplementary data

FEA results and imposed boundary conditions to obtain the mechanical properties and Video captions of the tested samples.

Supplementary material related to this article can be found online at https://doi.org/10.1016/j.ijmecsci.2022.107741. Video A: Deformation of optimum structure in compression (magnification = 1500X, voltage = 2 kV, beam current = 0.2 nA).

Video B: Deformation of optimum structure in shear (magnification = 1200X, voltage = 2 kV, beam current = 0.2 nA).

Supplementary Information: Details about Figure S1 and Figure S2. The data needed to evaluate the conclusions in the paper are present

The data needed to evaluate the conclusions in the paper are prese in the paper and/or the Supplementary Materials.

References

- Geng Qiang, Wang Dien, Chen Pengfei, Chen Shih-Chi. Ultrafast multi-focus 3-D nano-fabrication based on two-photon polymerization. Nature Commun 2019;10:2179.
- [2] Jonušauskas Linas, Gailevičius Darius, Rekštytė Sima, Baldacchini Tommaso, Juodkazis Saulius, Malinauskas Mangirdas. Mesoscale laser 3D printing. Opt Express 2019;27(11):15205–21.
- [3] Somers Paul, Liang Zihao, Johnson Jason E, Boudouris Bryan W, Pan Liang, Xu Xianfan. Rapid, continuous projection multi-photon 3D printing enabled by spatiotemporal focusing of femtosecond pulses. Light: Sci Appl 2021;10(1):1–11.
- [4] Surjadi James Utama, Gao Libo, Du Huifeng, Li Xiang, Xiong Xiang, Fang Nicholas Xuanlai, Lu Yang. Mechanical metamaterials and their engineering applications. Adv Energy Mater 2019;21(3):1800864.
- [5] Pham Minh-Son, Liu Chen, Todd Iain, Lertthanasarn Jedsada. Damagetolerant architected materials inspired by crystal microstructure. Nature 2019;565(7739):305–11.
- [6] Zhang Xuan, Vyatskikh Andrey, Gao Huajian, Greer Julia R, Li Xiaoyan. Lightweight, flaw-tolerant, and ultrastrong nanoarchitected carbon. Proc Natl Acad Sci 2019;116(14).
- [7] Meza Lucas R, Das Satyajit, Greer Julia R. Strong, lightweight, and recoverable three-dimensional ceramic nanolattices. Science 2014.
- [8] Zheng Xiaoyu, Lee Howon, Weisgraber Todd H, Shusteff Maxim, DeOtte Joshua, Duoss Eric B, Kuntz Joshua D, Biener Monika M, Ge Qi, Jackson Julie A, Kucheyev Sergei O, Fang Nicholas X, Spadaccini Christopher M. Ultralight, ultrastiff mechanical metamaterials. Science 2014.
- [9] Cui Huachen, Hensleigh Ryan, Yao Desheng, Maurya Deepam, Kumar Prashant, Kang Min Gyu, Priya Shashank, Zheng Xiaoyu (Rayne). Three-dimensional printing of piezoelectric materials with designed anisotropy and directional response. Nature Mater 2019;18(3).
- [10] Xia Xiaoxing, Afshar Arman, Yang Heng, Portela Carlos M, Kochmann Dennis M, Di Leo Claudio V, Greer Julia R. Electrochemically reconfigurable architected materials. Nature 2019;573(7773).
- [11] Song Jian, Zhou Wenzhao, Wang Yuejiao, Fan Rong, Wang Yinchu, Chen Junying, Lu Yang, Li Lixiao. Octet-truss cellular materials for improved mechanical properties and specific energy absorption. Mater Des 2019;173:107773.
- [12] Vangelatos Zacharias, Sheikh Haris Moazam, Marcus Philip S, Grigoropoulos Costas P, Lopez Victor Z, Flamourakis George, Farsari Maria. Strength through defects: A novel Bayesian approach for the optimization of architected materials. Sci Adv 2021:7(41).
- [13] Beli D, Arruda JRF, Ruzzene M. Wave propagation in elastic metamaterial beams and plates with interconnected resonators. Int J Solids Struct 2018;139:105–20.
- [14] Huang Jijie, Jin Tiening, Misra Shikhar, Wang Han, Qi Zhimin, Dai Yaomin, Sun Xing, Li Leigang, Okkema Joseph, Chen Hou-Tong, et al. Tailorable optical response of Au-LiNbO3 hybrid metamaterial thin films for optical waveguide applications. Adv Opt Mater 2018;6(19):1800510.
- [15] Yin Sha, Guo Weihua, Wang Huitian, Huang Yao, Yang Ruiheng, Hu Zihan, Chen Dianhao, Xu Jun, Ritchie Robert O. Strong and tough bioinspired additivemanufactured dual-phase mechanical metamaterial composites. J Mech Phys Solids 2021;149:104341.
- [16] Jia Zian, Fernandes Matheus C, Deng Zhifei, Yang Ting, Zhang Qiuting, Lethbridge Alfie, Yin Jie, Lee Jae-Hwang, Han Lin, Weaver James C, et al. Microstructural design for mechanical-optical multifunctionality in the exoskeleton of the flower beetle torynorrhina flammea. Proc Natl Acad Sci 2021;118(25).
- [17] Huang Lingxi, Duan Yuping, Liu Jia, Zeng Yuansong, Ma Guojia, Pang Huifang, Gao Shaohua, Zhang Weiping. Bioinspired gyrotropic metamaterials with multifarious wave adaptability and multifunctionality. Adv Opt Mater 2020;8(12):2000012.
- [18] Fernandes Matheus C, Aizenberg Joanna, Weaver James C, Bertoldi Katia. Mechanically robust lattices inspired by deep-sea glass sponges. Nature Mater 2021;20(2):237–41.
- [19] Pham Minh-Son, Liu Chen, Todd Iain, Lertthanasarn Jedsada. Damagetolerant architected materials inspired by crystal microstructure. Nature 2019;565(7739):305–11.
- [20] Gross Andrew, Pantidis Panos, Bertoldi Katia, Gerasimidis Simos. Correlation between topology and elastic properties of imperfect truss-lattice materials. J Mech Phys Solids 2019;124:577–98.
- [21] Derveni Fani, Gross Andrew J, Peterman Kara D, Gerasimidis Simos. Postbuckling behavior and imperfection sensitivity of elastic-plastic periodic plate-lattice materials. Extreme Mech Lett 2022;50:101510.
- [22] Schwaiger R, Meza LR, Li X. The extreme mechanics of micro- and nanoarchitected materials. MRS Bull 2019;44(10):758-65.
- [23] Al-Ketan Oraib, Rezgui Rachid, Rowshan Reza, Du Huifeng, Fang Nicholas X, Abu Al-Rub Rashid K. Microarchitected stretching-dominated mechanical metamaterials with minimal surface topologies. Adv Energy Mater 2018;20(9).
- [24] Ashby Michael F. The properties of foams and lattices. Phil Trans R Soc A 2006;364(1838):15–30.
- [25] Tancogne-Dejean Thomas, Spierings Adriaan B, Mohr Dirk. Additively-manufactured metallic micro-lattice materials for high specific energy absorption under static and dynamic loading. Acta Mater 2016;116:14–28.

- [26] Portela Carlos M, Vidyasagar A, Krödel Sebastian, Weissenbach Tamara, Yee Daryl W, Greer Julia R, Kochmann Dennis M. Extreme mechanical resilience of self-assembled nanolabyrinthine materials. Proc Natl Acad Sci 2020;117(11):5686–93.
- [27] Bastek Jan-Hendrik, Kumar Siddhant, Telgen Bastian, Glaesener Raphaël N, Kochmann Dennis M. Inverting the structure–property map of truss metamaterials by deep learning. Proc Natl Acad Sci 2022;119(1).
- [28] Zheng Li, Kumar Siddhant, Kochmann Dennis M. Data-driven topology optimization of spinodoid metamaterials with seamlessly tunable anisotropy. Comput Methods Appl Mech Engrg 2021;383:113894.
- [29] Ma Qingping, Zhang Lei, Ding Junhao, Qu Shuo, Fu Jin, Zhou Mingdong, Fu Ming Wang, Song Xu, Wang Michael Yu. Elastically-isotropic open-cell minimal surface shell lattices with superior stiffness via variable thickness design. Addit Manuf 2021;47:102293.
- [30] Ma Qingping, Yan Zhenjun, Zhang Lei, Wang Michael Yu. The family of elastically isotropic stretching-dominated cubic truss lattices. Int J Solids Struct 2022;111451.
- [31] Feng Jiawei, Liu Bo, Lin Zhiwei, Fu Jianzhong. Isotropic porous structure design methods based on triply periodic minimal surfaces. Mater Des 2021;210:110050.
- [32] Lei Ming, Hong Wei, Zhao Zeang, Hamel Craig, Chen Mingji, Lu Haibao, Qi H Jerry. 3D printing of auxetic metamaterials with digitally reprogrammable shape. ACS Appl Mater Interfaces 2019;11(25):22768–76.
- [33] Shen Jianhu, Zhou Shiwei, Huang Xiaodong, Xie Yi Min. Simple cubic threedimensional auxetic metamaterials. Phys Status Solidi (B) 2014;251(8):1515–22.
- [34] Zheng Xiaoyu, Lee Howon, Weisgraber Todd H, Shusteff Maxim, DeOtte Joshua, Duoss Eric B, Kuntz Joshua D, Biener Monika M, Ge Qi, Jackson Julie A, et al. Ultralight, ultrastiff mechanical metamaterials. Science 2014;344(6190):1373–7.
- [35] Khajehtourian Romik, Kochmann Dennis M. A continuum description of substrate-free dissipative reconfigurable metamaterials. J Mech Phys Solids 2021;147:104217.
- [36] Spagnuolo Mario, Yildizdag M Erden, Andreaus Ugo, Cazzani Antonio M. Are higher-gradient models also capable of predicting mechanical behavior in the case of wide-knit pantographic structures? Math Mech Solids 2021;26(1):18–29.
- [37] Agrawal Gourav, Gupta Abhinav, Chowdhury Rajib, Chakrabarti Anupam. Robust topology optimization of negative Poisson's ratio metamaterials under material uncertainty. Finite Elem Anal Des 2022;198:103649.
- [38] Chang Yafeng, Wang Hui, Dong Qinxi. Machine learning-based inverse design of auxetic metamaterial with zero Poisson's ratio. Mater Today Commun 2022:103186.
- [39] Jiang Weifeng, Zhu Yangyang, Yin Guofu, Lu Houhong, Xie Luofeng, Yin Ming. Dispersion relation prediction and structure inverse design of elastic metamaterials via deep learning. Mater Today Phys 2022;100616.
- [40] Bacigalupo Andrea, Gnecco Giorgio, Lepidi Marco, Gambarotta Luigi. Machine-learning techniques for the optimal design of acoustic metamaterials. J Optim Theory Appl 2020;187(3):630–53.
- [41] Challapalli Adithya, Patel Dhrumil, Li Gouqiang. Inverse machine learning framework for optimizing lightweight metamaterials. Mater Des 2021;208:109937.
- [42] Garland Anthony P, White Benjamin C, Jensen Scott C, Boyce Brad L. Pragmatic generative optimization of novel structural lattice metamaterials with machine learning. Mater Des 2021;203:109632.
- [43] Dos Reis Francisco, Karathanasopoulos Nikolaos. Inverse metamaterial design combining genetic algorithms with asymptotic homogenization schemes. Int J Solids Struct 2022;250:111702.
- [44] Bessa Miguel A, Glowacki Piotr, Houlder Michael. Bayesian machine learning in metamaterial design: fragile becomes supercompressible. Adv Mater 2019;31(48):1904845.
- [45] Matthews Jordan, Klatt Timothy, Morris Clinton, Seepersad Carolyn C, Haberman Michael, Shahan David. Hierarchical design of negative stiffness metamaterials using a bayesian network classifier. J Mech Des 2016;138(4).
- [46] Sharpe Conner, Seepersad Carolyn Conner, Watts Seth, Tortorelli Dan. Design of mechanical metamaterials via constrained bayesian optimization. In: ASME 2018 international design engineering technical conferences and computers and information in engineering conference. American Society of Mechanical Engineers Digital Collection; 2018.
- [47] Vangelatos Z, Komvopoulos K, Grigoropoulos CP. Vacancies for controlling the behavior of microstructured three-dimensional mechanical metamaterials. Math Mech Solids 2019;24(2):511–24.
- [48] Deshpande Vikram S, Fleck Norman A, Ashby Michael F. Effective properties of the octet-truss lattice material. J Mech Phys Solids 2001;49(8):1747–69.
- [49] Viterbo Emanuele, Biglieri Ezio. Computing the voronoi cell of a lattice: the diamond-cutting algorithm. IEEE Trans Inform Theory 1996;42(1):161–71.
- [50] Clayton John D. Nonlinear mechanics of crystals, Vol. 177. Springer Science & Business Media; 2010.
- [51] Ming Pingbing, et al. Cauchy–Born rule and the stability of crystalline solids: static problems. Arch Ration Mech Anal 2007;183(2):241–97.
- [52] Ericksen JL. On the Cauchy—Born rule. Math Mech Solids 2008;13(3-4):199– 220.
- [53] Aghaei A, Qomi MJ Abdolhosseini, Kazemi MT, Khoei AR. Stability and size-dependency of Cauchy–Born hypothesis in three-dimensional applications. Int J Solids Struct 2009;46(9):1925–36.

- [54] Sheikh Haris Moazam, Marcus Philip S. Bayesian optimization for multi-objective mixed-variable problems. 2022, URL http://arxiv.org/abs/2201.12767.
- [55] Lee Wooju, Kang Da-Young, Song Jihwan, Moon Jun Hyuk, Kim Dongchoul. Controlled unusual stiffness of mechanical metamaterials. Sci Rep 2016;6(1):1–7.
- [56] Gibson Lorna J, Ashby Michael F. Cellular solids: structure and properties. Cambridge University Press; 1999.
- [57] Brochu Eric, Cora Vlad M, de Freitas Nando. A tutorial on Bayesian optimization of expensive cost functions, with application to active user modeling and hierarchical reinforcement learning. 2010.
- [58] Frazier Peter I, Wang Jialei. Bayesian optimization for materials design. Springer series in materials science, Springer International Publishing; 2015, p. 45–75.
- [59] Chen Desai, Skouras Mélina, Zhu Bo, Matusik Wojciech. Computational discovery of extremal microstructure families. Sci Adv 2018;4(1):eaao7005.
- [60] Chen Wen, Watts Seth, Jackson Julie A, Smith William L, Tortorelli Daniel A, Spadaccini Christopher M. Stiff isotropic lattices beyond the maxwell criterion. Sci Adv 2019;5(9):eaaw1937.
- [61] Shaw Lucas A, Sun Frederick, Portela Carlos M, Barranco Rodolfo I, Greer Julia R, Hopkins Jonathan B. Computationally efficient design of directionally compliant metamaterials. Nature Commun 2019;10(1):1–13.
- [62] Song Jian, Wang Yuejiao, Zhou Wenzhao, Fan Rong, Yu Bin, Lu Yang, Li Lixiao. Topology optimization-guided lattice composites and their mechanical characterizations. Composites B 2019;160:402–11.
- [63] Snoek Jasper, Larochelle Hugo, Adams Ryan P. Practical Bayesian optimization of machine learning algorithms. 2012.
- [64] Chen Yutian, Huang Aja, Wang Ziyu, Antonoglou Ioannis, Schrittwieser Julian, Silver David, de Freitas Nando. Bayesian optimization in alphago. 2018, CoRR abs/1812.06855. URL http://arxiv.org/abs/1812.06855.
- [65] Oh ChangYong, Gavves Efstratios, Welling Max. BOCK: Bayesian optimization with cylindrical kernels. In: Proceedings of the 35th international conference on machine learning. Proceedings of machine learning research, vol. 80, PMLR; 2018, p. 3868–77.
- [66] Pyzer-Knapp Edward. Bayesian optimization for accelerated drug discovery. IBM J Res Dev 2018;PP:1.
- [67] Korovina Ksenia, Xu Sailun, Kandasamy Kirthevasan, Neiswanger Willie, Poczos Barnabas, Schneider Jeff, Xing Eric. ChemBO: Bayesian optimization of small organic molecules with synthesizable recommendations. In: Proceedings of the twenty third international conference on artificial intelligence and statistics. Proceedings of machine learning research, vol. 108, PMLR; 2020, p. 3393–403.
- [68] Mockus J. Application of Bayesian approach to numerical methods of global and stochastic optimization. J Global Optim 1994;4:347–65.
- [69] Xu Shanqing, Shen Jianhu, Zhou Shiwei, Huang Xiaodong, Xie Yi Min. Design of lattice structures with controlled anisotropy. Mater Des 2016;93:443–7.
- [70] Brochu Eric, Hoffman Matthew W, de Freitas Nando. Portfolio allocation for Bayesian optimization. 2011.

- [71] Tušar Tea, Brockhoff Dimo, Hansen Nikolaus. Mixed-integer benchmark problems for single- and bi-objective optimization. In: Proceedings of the genetic and evolutionary computation conference. GECCO '19, New York, NY, USA: Association for Computing Machinery; 2019, p. 718–26.
- [72] Norris Andrew N. Poisson's ratio in cubic materials. Proc R Soc Lond Ser A Math Phys Eng Sci 2006;462(2075):3385–405.
- [73] Yamawaki Masaki, Ohnishi Masato, Ju Shenghong, Shiomi Junichiro. Multifunctional structural design of graphene thermoelectrics by Bayesian optimization. Sci Adv 2018;4(6).
- [74] Gongora Aldair E, Xu Bowen, Perry Wyatt, Okoye Chika, Riley Patrick, Reyes Kristofer G, Morgan Elise F, Brown Keith A. A Bayesian experimental autonomous researcher for mechanical design. Sci Adv 2020;6(15).
- [75] Yamashita Tomoki, Sato Nobuya, Kino Hiori, Miyake Takashi, Tsuda Koji, Oguchi Tamio. Crystal structure prediction accelerated by Bayesian optimization. Phys Rev Mater 2018;2(1):013803.
- [76] Zanzotto Giovanni. The Cauchy–Born hypothesis, nonlinear elasticity and mechanical twinning in crystals. Acta Crystallogr Sect A: Found Crystallogr 1996:52(6):839–49.
- [77] Cocco Giulio, Cadelano Emiliano, Colombo Luciano. Gap opening in graphene by shear strain. Phys Rev B 2010;81(24):241412.
- [78] Iglesias Martínez Julio Andrés, Moughames Johnny, Ulliac Gwenn, Kadic Muamer, Laude Vincent. Three-dimensional phononic crystal with ultra-wide bandgap at megahertz frequencies. Appl Phys Lett 2021:118(6):063507.
- [79] Kumar Ajeet, Kumar Siddhant, Gupta Prakhar. A helical Cauchy-Born rule for special cosserat rod modeling of nano and continuum rods. J Elasticity 2016;124(1):81–106.
- [80] Yildizdag Mustafa Erden, Tran Chuong Anthony, Barchiesi Emilio, Spagnuolo Mario, Hild François, et al. A multi-disciplinary approach for mechanical metamaterial synthesis: a hierarchical modular multiscale cellular structure paradigm. In: State of the art and future trends in material modeling. Springer; 2019. p. 485–505.
- [81] Yildizdag M Erden, Barchiesi Emilio, dell'Isola Francesco. Three-point bending test of pantographic blocks: numerical and experimental investigation. Math Mech Solids 2020;25(10):1965–78.
- [82] Moestopo Widianto P, Mateos Arturo J, Fuller Ritchie M, Greer Julia R, Portela Carlos M. Pushing and pulling on ropes: hierarchical woven materials. Adv Sci 2020:7(20):2001271.
- [83] Arroyo Marino, Belytschko Ted. An atomistic-based finite deformation membrane for single layer crystalline films. J Mech Phys Solids 2002;50(9):1941–77.